Geophys. J. Int. (1999) **138,** 205–220

Resolving power of surface wave polarization data for higher-order heterogeneities

Kazunori Yoshizawa,[1,*] Kiyoshi Yomogida[1,†] and Seiji Tsuboi[2]

[1] *Department of Earth and Planetary Systems Science, Hiroshima University, Higashi-Hiroshima* 739-8526, *Japan*
[2] *Department of Geoscience, National Defense Academy, Yokosuka* 239-8686, *Japan*

Accepted 1999 February 15. Received 1999 February 10; in original form 1998 August 6

SUMMARY

The resolving power of polarization data compared with that of phase data is investigated by employing both synthetic and observed data sets, using the linear relationship between the phase velocity perturbation and the phase or polarization anomaly. In order to investigate the intrinsic differences between phase and polarization data, a synthetic test is first undertaken using a white noise model with sufficiently uniform coverage of ray paths. This test shows that polarization data can retrieve higher-order heterogeneities of degrees up to 20 almost completely, despite damping and smoothing effects, whilst phase data can only retrieve those of degrees lower than 8 with reasonable damping. Next, about 4000 phase and 2500 polarization records are collected for minor- and major-arc Rayleigh waves (R1 and R2) in the frequency range 4–12 mHz. To correct the Rayleigh wave polarization data, the misorientation of each station is estimated from the polarization of long-period *P* waves propagating mainly in the lower mantle. The phase and polarization data are then inverted for the phase velocity distribution in spherical harmonics with degrees up to 15. The phase velocity maps derived from the phase data are quite consistent with previous studies, whilst those from the polarization data show some discrepancies. For example, the correlation between the phase and polarization models is quite good for low even degrees such as 2, 4 and 6, but not for low odd degrees or degrees higher than 8. The gradients of amplitude spectra from the polarization data are smaller than those from the phase data, especially at degrees higher than 6, which suggests a slightly higher sensitivity of the polarization data to higher-order heterogeneities. Nevertheless, the overall spectral characteristics of both models are similar; that is, low-order heterogeneities are dominant whilst higher orders are clearly reduced. Further investigation using a synthetic test with the same uneven paths as the observed data shows the suppression of higher-order heterogeneities. Since the synthetic test with even paths retrieves higher-order heterogeneities sufficiently, this result strongly suggests the path averaging effect of uneven ray paths that is intrinsic in the ray theoretical approach used in this study as well as almost all the global inversions. Although inversions based on geometrical ray theory have some limited resolving power with the current status of global records, polarization data are indeed helpful in resolving higher-order lateral heterogeneities with the dense and uniform path coverage that is becoming available.

Key words: lateral heterogeneity, polarization, ray theory, surface waves, tomography.

1 INTRODUCTION

The global velocity structure of the Earth's interior is a key factor in investigating its internal evolution and ongoing processes such as mantle convection. For obtaining a detailed image of the Earth's interior, seismic tomography is the most powerful tool, and has been widely used to investigate global and local lateral heterogeneities of the Earth since the 1980s. Although the quality of recorded seismograms has improved and their number has increased since the beginning of global velocity inversions, almost all researchers have used the same kind of data; that is, the phase-delay information: traveltime for body waves (Dziewonski 1984; Inoue *et al.* 1990; Kennett

*Now at: Research School of Earth Sciences, the Australian National University, Canberra ACT 0200, Australia. E-mail: kazu@rses.anu.edu.au
†Now at: Division of Earth and Planetary Sciences, Hokkaido University, Sapporo 060-0810, Japan.

et al. 1998) or phase shift for surface waves (Nakanishi & Anderson 1983, 1984; Tanimoto & Anderson 1985; Tanimoto 1990; Montagner & Tanimoto 1990; Trampert & Woodhouse 1995; Zhang & Lay 1996; Ekström *et al.* 1997). This situation has not changed, even though some researchers used waveforms of body or surface waves (Woodhouse & Dziewonski 1984; Honda & Tanimoto 1987; Su *et al.* 1994), since they perturbed only the phase part of waveforms. Exceptions were found only in several works with amplitude data (Yomogida & Aki 1987; Neele *et al.* 1993; Laske & Masters 1996).

If a medium contains lateral heterogeneities, not only is the phase of the surface wave varied but also its polarization plane deviates from the great-circle path (Lay & Kanamori 1985; Yomogida & Aki 1987; Laske *et al.* 1994; Laske 1995), as shown in Fig. 1. Following Woodhouse & Wong (1986) and Yanovskaya (1996), the perturbation of a polarization plane, $\delta\alpha$ ($= \tan\Theta_{\rm H}$, where $\Theta_{\rm H}$ is the arrival angle), is linearly related to the gradient of phase velocity perturbation δc perpendicular to the great-circle path:

$$\delta\alpha \simeq -\int_0^{\Delta} \frac{\sin s}{\sin\Delta}\frac{\partial}{\partial \mathbf{n}_0}\left(\frac{\delta c(\theta,\varphi)}{c_0}\right) ds\,, \tag{1}$$

where Δ is the epicentral distance, $\mathbf{n}_0$ is the unit vector perpendicular to the great-circle path, c_0 is the reference phase velocity and ds is the ray path increment along the great circle (Fig. 1). The integration along the actual ray path from source to receiver can be approximated by the integration along the great circle if the velocity perturbation is smooth enough (Yanovskaya 1996). In contrast, the widely used phase perturbation $\delta\psi$ is related to the phase velocity perturbation δc itself:

$$\delta\psi \simeq -k\int_0^{\Delta} \frac{\delta c(\theta,\varphi)}{c_0} ds\,, \tag{2}$$

where k is the wavenumber. Thus polarization data should hold greater resolving power for phase velocity variations than phase data, although phase data are more robust against noise in the data and insufficient coverage of ray paths. Using polarization anomalies, we may obtain models with different resolution characteristics from those of previous models. The recent study of Laske & Masters (1996) showed that phase velocity maps derived from both phase and polarization data are significantly improved in the resolution of higher-order heterogeneities, compared with those only from phase data.

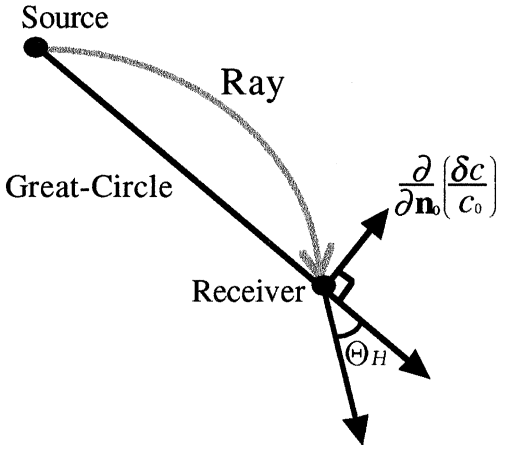

Figure 1. Geometry of a ray propagating in a heterogeneous medium. $\Theta_{\rm H}$ is the polarization angle at an observation point. Polarization anomalies are sensitive to the gradient of phase velocity perturbation, δc, perpendicular to the ray path, $\mathbf{n}_0$.

In this study, we first perform a synthetic test with a white noise model to visualize the sensitivity of phase and polarization data to higher-order heterogeneities. In order to investigate the difference between the two data sets, we perform linear inversions with phase and polarization data independently. It is beyond the scope of this study to propose a new global phase velocity model or to perform a joint inversion of phase and polarization data, although it would be possible to undertake. We then invert observed Rayleigh wave phase and polarization data in the frequency range 4–12 mHz. We use only fundamental-mode Rayleigh waves, not Love waves, because fundamental-mode Love waves at periods around 100 s are likely to be contaminated by their first higher mode (e.g. Thatcher & Brune 1969; Boore 1969; Dziewonski *et al.* 1972; Nakanishi & Anderson 1984). We also discuss the station correction which is critical for polarization data inversions. The polarization anomaly or arrival angle is measured as the deviation from the radial direction, but if horizontal components at a station are not oriented accurately, we cannot obtain reliable arrival angles. We estimate the misorientation of each station from *P*-wave polarization data and correct Rayleigh wave arrival angles. We finally discuss the sensitivity of polarization data to higher-order heterogeneities, using inverted models with actual phase and polarization data, and their implications for the limit of geometrical ray theory to resolve higher-order heterogeneities.

2 FORMULATION OF LINEAR INVERSION

The phase velocity perturbation $\delta c(\theta, \phi)$ with respect to the reference velocity c_0 is expanded in fully normalized spherical harmonics,

$$\frac{\delta c(\theta,\phi)}{c_0} = \sum_{l=1}^{L}\sum_{m=0}^{l} c_l^m (A_l^m \cos m\varphi + B_l^m \sin m\varphi) P_l^m(\cos\theta)\,, \tag{3}$$

$$c_l^m = \left[(2l+1)(2-\delta_{m,0})\frac{(l-m)!}{(l+m)!}\right]^{1/2}, \tag{4}$$

where L is the maximum order of the expansion, A_l^m and B_l^m are the coefficients of spherical harmonics of orders l and m and P_l^m is the associated Legendre function. In order to simplify the integration along a great circle in eq. (1) or (2), we rotate the spherical harmonics in (3) by introducing a new coordinate system (θ', φ') so that the great-circle path is located on the equator (e.g. Backus 1964; Dziewonski 1984; Doornbos 1988). In this new coordinate, eqs (1) and (2) are represented as follows:

$$\delta\alpha \simeq -\frac{1}{\sin\Delta}\int_0^{\Delta} \sin\varphi' \frac{\partial}{\partial\theta'}\left(\frac{\delta c\left(\frac{\pi}{2},\varphi'\right)}{c_0}\right) d\varphi'\,, \tag{5}$$

$$\delta\psi \simeq -\frac{\omega a}{c_0}\int_0^{\Delta} \frac{\delta c\left(\frac{\pi}{2},\varphi'\right)}{c_0}\, d\varphi'\,, \tag{6}$$

where a is the Earth's radius and ω is the angular frequency. We can then integrate (5) or (6) analytically, since the integration is only for φ'.

Observed data are related to model parameters by

$$\mathbf{d}=\mathbf{G}\mathbf{m}+\mathbf{n}, \tag{7}$$

where $\mathbf{d}$ is the data vector ($\delta\psi$ or $\delta\alpha$ in this case), $\mathbf{G}$ is the kernel matrix, which consists of the right-hand side in (5) or (6) except for coefficients of spherical harmonics, $\mathbf{m}$ is the model parameter vector (A_l^m and B_l^m) and $\mathbf{n}$ is the noise vector. Our inversion scheme is based on damped least squares (e.g. Aki & Richards 1980), minimizing the following quantity:

$$\Phi=(\mathbf{d}-\mathbf{G}\mathbf{m})^{\mathrm{T}}(\mathbf{d}-\mathbf{G}\mathbf{m})+\varepsilon^2\mathbf{m}^{\mathrm{T}}\mathbf{D}^{\mathrm{T}}\mathbf{D}\mathbf{m}, \tag{8}$$

where ε^2 is the damping parameter and $\mathbf{R}_{\mathrm{m}}=(\mathbf{D}^{\mathrm{T}}\mathbf{D})^{-1}$ is the model covariance matrix to smooth the model space. The estimated model vector then becomes

$$\hat{\mathbf{m}}=(\mathbf{G}^{\mathrm{T}}\mathbf{G}+\varepsilon^2\mathbf{R}_{\mathrm{m}}^{-1})^{-1}\mathbf{G}^{\mathrm{T}}\mathbf{d}. \tag{9}$$

To evaluate how the solution fits the data, we calculate the following data misfit function:

$$\chi^2=\sum_{i=1}^{N}\left(\frac{d_i-\sum_{j=1}^{M}G_{ij}m_j}{n_i}\right)^2, \tag{10}$$

where N and M are the total numbers of data and model parameters, respectively, and n_i is the estimated error in the ith datum. The error estimations are briefly discussed in a later section.

In the case of expanding the phase velocity distribution in spherical harmonics, we must truncate them at a certain degree limit (L in 3), 20 for the synthetic test and 15 for the actual data inversion in this study, which leads to some unwanted effects on an inverted model, especially on higher-order coefficients (e.g. Trampert & Woodhouse 1995). In order to prevent this phenomenon, we take the roughness of model parameters, $\mathcal{R}=\|\mathbf{D}\mathbf{m}\|$, into consideration. Some researchers take it as the root mean square (rms) Laplacian of velocity perturbations (e.g. Trampert & Woodhouse 1995; Laske & Masters 1996),

$$\mathcal{R}\propto\left[\int_{\Omega}\left|\nabla^2\frac{\delta c(\theta,\varphi)}{c_0}\right|^2 d\Omega\right]^{1/2}, \tag{11}$$

where Ω is the surface of the Earth, and others use the rms gradient (Ekström *et al.* 1997),

$$\mathcal{R}\propto\left[\int_{\Omega}\left|\nabla\frac{\delta c(\theta,\varphi)}{c_0}\right|^2 d\Omega\right]^{1/2}. \tag{12}$$

The matrix $\mathbf{R}_{\mathrm{m}}^{-1}$ then becomes $l^2(l+1)^2\mathbf{I}$ for (11) and $l(l+1)\mathbf{I}$ for (12). The choice of $\mathcal{R}$ especially affects the higher-order coefficients; that is, the roughness of (11) tends to suppress higher-order heterogeneities more than (12). We perform preliminary inversions with the above two roughnesses and plot the normalized misfit, χ^2/N, against the normalized model roughness, $\|\mathbf{D}\mathbf{m}\|^2/\|\mathbf{D}\|^2$, but there is no remarkable difference between them. Since polarization data should be more sensitive to higher-order heterogeneities than conventional phase data, we prefer the roughness parameter (12), which does not suppress higher orders so much. For all the inversions in this study, we define the roughness parameter as

$$\mathcal{R}^2=\sum_{l=1}^{L}l(l+1)\sum_{m=0}^{l}[(A_l^m)^2+(B_l^m)^2]. \tag{13}$$

We draw a trade-off curve in the diagram of normalized data misfit χ^2/N versus squared model roughness $\mathcal{R}^2$ and choose the most reasonable damping parameter that is the closest to the origin of this diagram (Fig. 2).

3 WHITE NOISE SYNTHETIC TEST

In order to investigate the intrinsic resolving power of phase and polarization data, we first perform a test with a 'white noise model', which consists of constant-amplitude spectra $X(l)$ at all degrees:

$$X(l)=\left[\frac{\sum_{m=0}^{l}[(A_l^m)^2+(B_l^m)^2]}{2l+1}\right]^{1/2}, \tag{14}$$

with random spectral phases. The synthesized model (Fig. 3a) contains completely flat spectra up to degrees 20, so it is useful to check the spectral characteristics of a retrieved model from phase or polarization data. We set sufficiently dense and even path coverage, which consists of about 4600 synthetic source–receiver pairs corresponding to minor-arc waves (R1 or G1). We calculate the synthetic phase and polarization data ($\delta\psi$ and $\delta\alpha$, respectively) by integrating the phase velocity perturbations of the white noise model along the great circle using (1) and (2). To investigate the intrinsic difference between phase and polarization data, we use the smoothing filter discussed in the previous section. The damping parameter ε^2 is 1.0 for both phase and polarization tests to give the best trade-off compromise.

Retrieved maps and spectra are shown in Fig. 3. Both phase and polarization data retrieve the overall features of the white noise model well. The most significant difference between the retrieved maps appears in the higher-order terms, especially higher than degree 8. Amplitude spectra from phase data

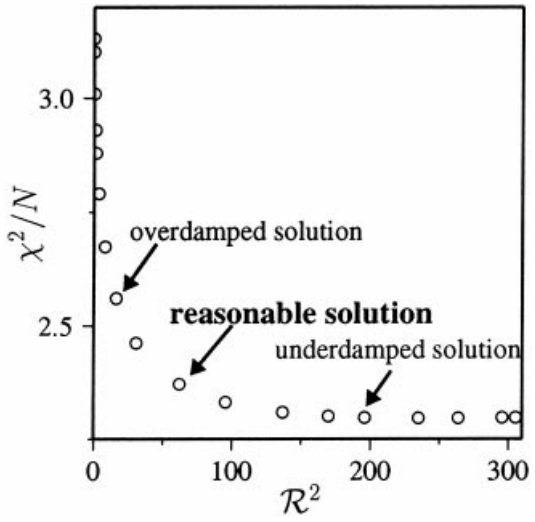

Figure 2. Trade-off curve for polarization data inversion at period 152 s.

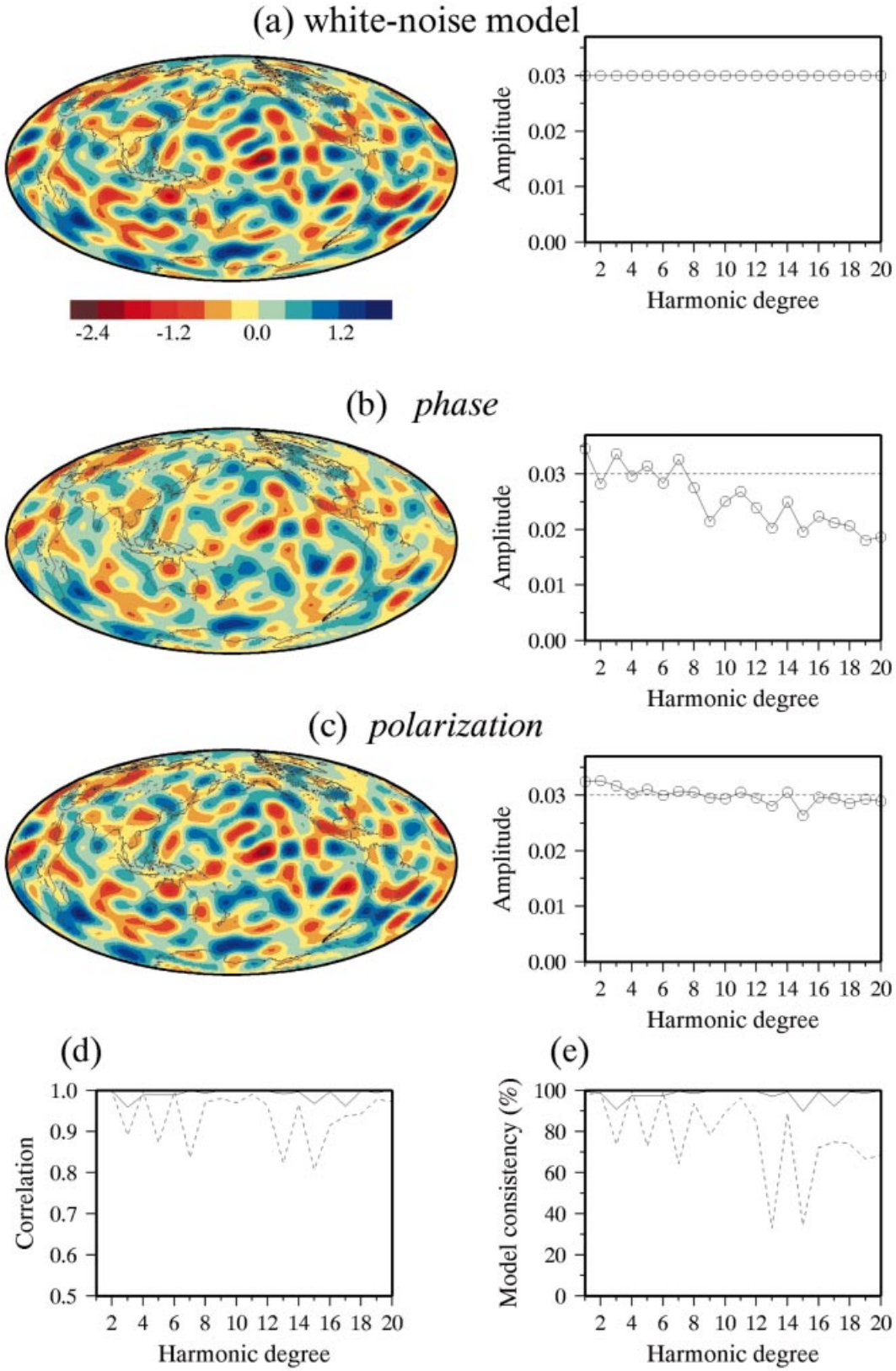

Figure 3. (a) White noise model of phase velocity and their spectra. Retrieved maps and amplitude spectra from (b) synthetic phase data and (c) synthetic polarization data with sufficiently dense and even path coverage. (d) Correlation coefficients and (e) model consistency between the original model (a) and the retrieved models (b or c) from phase data (dotted line) and polarization data (solid line). Note that the minimum value in the ordinate of (d) is 0.5. Retrieved maps and amplitude spectra from (f) phase data and (g) polarization data synthesized for the actual path coverage of the observed phase data set (Fig. 4b). A dotted line in each amplitude diagram shows the flat amplitude of the original white noise model. Contour intervals of all retrieved maps are the same.

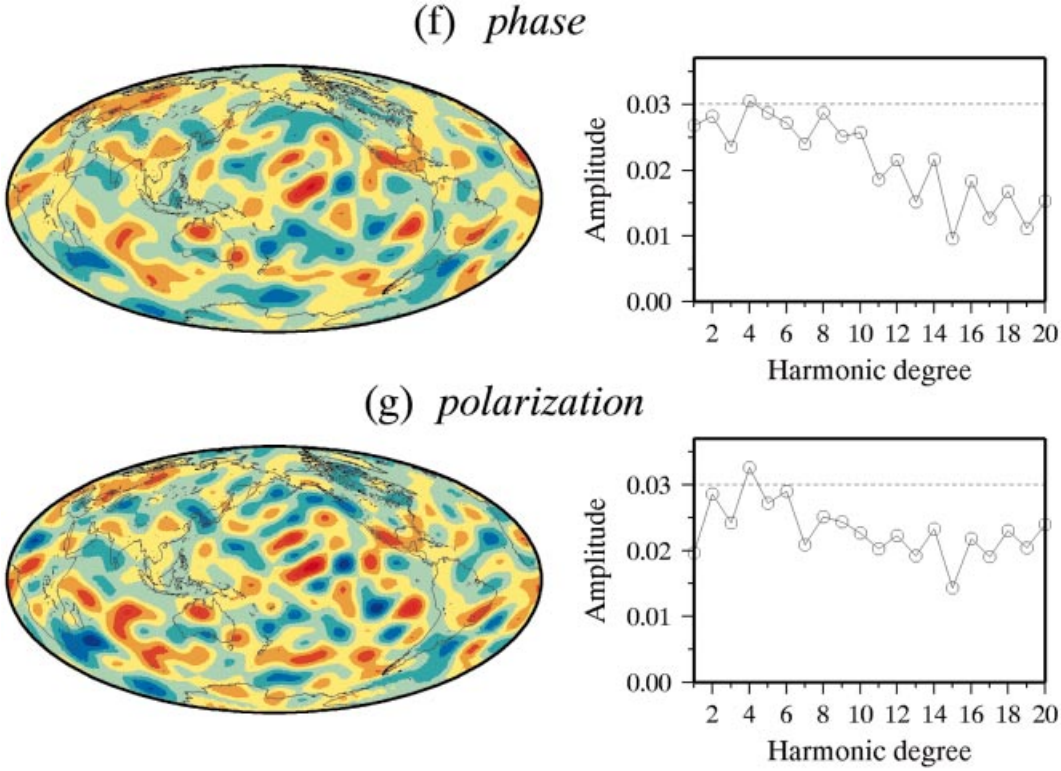

Figure 3. (*continued.*)

systematically fall off for degrees over 8, whilst those from polarization data are nearly flat, similar to the original. The correlations between the original white noise model and retrieved models from phase and polarization data are shown in Fig. 3(d). The correlation coefficients are more than 0.95 for the polarization data and more than 0.8 for the phase data at all degrees. Since the correlation coefficients are only sensitive to the agreement of model patterns, not to the differences in their amplitudes, we further evaluate the following model consistency (Hara *et al.* 1993) to quantify how well the model is retrieved:

$$\left[1-\frac{\int |c_{\rm in}(\theta,\phi)-c_{\rm out}(\theta,\phi)|^2\,d\Omega}{\sqrt{\int |c_{\rm in}(\theta,\phi)|^2\,d\Omega \int |c_{\rm out}(\theta,\phi)|^2\,d\Omega}}\right]\times 100\,, \qquad (15)$$

where $c_{\rm in}(\theta,\phi)$ is the phase velocity perturbation in the original or input model and $c_{\rm out}(\theta,\phi)$ is that in the retrieved or output model. The model consistency should be more suitable than the correlation coefficient for detecting slight differences between the two models. The total retrieval of the white noise model from the phase data is 84.8 per cent and that from the polarization data is 98.9 per cent. Fig. 3(e) shows the model consistency at each degree. Both the correlation coefficients and the model consistency share a common trend: they are smaller at odd degrees than at even degrees, especially for the phase model. Fig. 3(e) also shows that the model consistency for the phase model decreases with increasing degrees, whilst that for the polarization is almost constant, providing satisfactory retrieval of the original white noise model at all degrees.

We must note the following factors when we compare the above synthetic results with actual phase velocity models derived from observed data. We should retrieve the model thoroughly if we did not use any damping or smoothing in this synthetic test because data themselves are synthesized by the linear approximation (1 or 2) without noise and the coverage is sufficiently dense and uniform. In contrast, inversions with actual data need to be damped or smoothed because of uneven path coverage, incoherent noise in the data and truncation of spherical harmonics at a certain degree (Trampert & Woodhouse 1995). When we discuss higher-order heterogeneities, we must also pay attention to the limitations of the geometrical ray approximation (i.e. 1 and 2). The higher the order of the heterogeneities, the closer the considered wavelength becomes to the scale of heterogeneities. For example, the heterogeneity of degree 20 has a horizontal scale of about 2000 km, whilst the wavelength of the Rayleigh wave at periods of 200 s is greater than 800 km. The geometrical ray approximation therefore becomes less valid for long periods. As a result, higher-order heterogeneities may not be retrieved sufficiently, even if we use polarization data, as long as we blindly use this approximation, especially for long-period data. As the travel distance decreases, the geometrical ray approximation becomes relatively valid (see Section 13.3.5 of Aki & Richards 1980), so that only short paths such as R1 or G1 are required to retrieve small-scale heterogeneities.

4 PHASE AND POLARIZATION DATA

We collect three-component long-period seismograms of GSN stations in the data set IRIS FARM. Since we use polarization data; that is, a small signal in the transverse component of Rayleigh waves assumed to be caused by lateral heterogeneities, waveforms of surface waves must be clear. We must

also take care of the effect of higher-mode contamination. In order to collect high-quality fundamental-mode Rayleigh waves, we chose 152 events of surface wave magnitude greater than 6.5 and focal depth shallower than 100 km from 1990 to 1996. Global distributions of both the events and the stations used in this study are shown in Fig. 4(a). Minor-arc Rayleigh wave trains (R1) are overlapped by minor-arc Love wave trains (G1) at epicentral distances shorter than 50°, as are R2 by G3. We confine our data set in the range of epicentral distances larger than 50° not only for polarization data but also for phase data, although the phase data of Rayleigh waves could be analysed at much shorter distances. In order to investigate the intrinsic differences between phase and polarization data, it is better to collect data with identical criteria, although it results in smaller amounts of phase data than other state-of-the-art studies (e.g. Trampert & Woodhouse 1995; Zhang & Lay 1996; Ekström *et al.* 1997). The path coverage of phase and polarization data at a period of 152 s is shown in Fig. 4 and the number of data is listed in Table 1. The coverage is comparatively sparse for North and South Polar regions, the eastern region of Africa and the eastern Pacific, especially for polarization data.

All the seismograms are initially deconvolved to remove their instrument responses and compared with the corresponding synthetics calculated by employing the normal mode theory (Dziewonski & Woodhouse 1983) with a point source approximation. We use focal mechanism solutions of the Harvard centroid moment tensor inversion (e.g. Dziewonski *et al.* 1981) and PREM (Dziewonski & Anderson 1981) as a reference laterally homogeneous earth model. Through this comparison, some seismograms are discarded if they appear to be heavily contaminated with noise and some obvious errors in observation or if their stations are nearly located in a nodal direction of Rayleigh wave radiation, because they are quite sensitive to errors in the estimated source parameters.

An example of observed and corresponding synthetic seismograms of the vertical component is shown in Fig. 5(a). In the case of a laterally homogeneous earth, the Rayleigh wave propagates along the great-circle path, so that its particle motion is confined in the vertical–radial plane and does not appear in the transverse component. In contrast, as seen in Fig. 5(b), actual seismograms frequently have a small amount of the transverse component in the Rayleigh wave time window, which could be interpreted as the polarization anomaly due to lateral heterogeneities. In general, the measurement of polarization angles is more complicated than that of phase differences between the observed and synthetic seismograms. For instance, the measurement of the phase delay needs only one component (vertical in most cases, including this study), whereas the polarization measurement requires three components with excellent S/N ratio. Moreover, when we analyse polarization angles, we need to take a shorter time window than for the phase data to avoid the overlapping of Love wave in the transverse component. Furthermore, for polarization data we must intrinsically use amplitude information of all three components at each station, which greatly depends on the local site effect as well as the gain control quality of the seismometers. In spite of these difficulties, we manage to collect the polarization data with a high degree of accuracy.

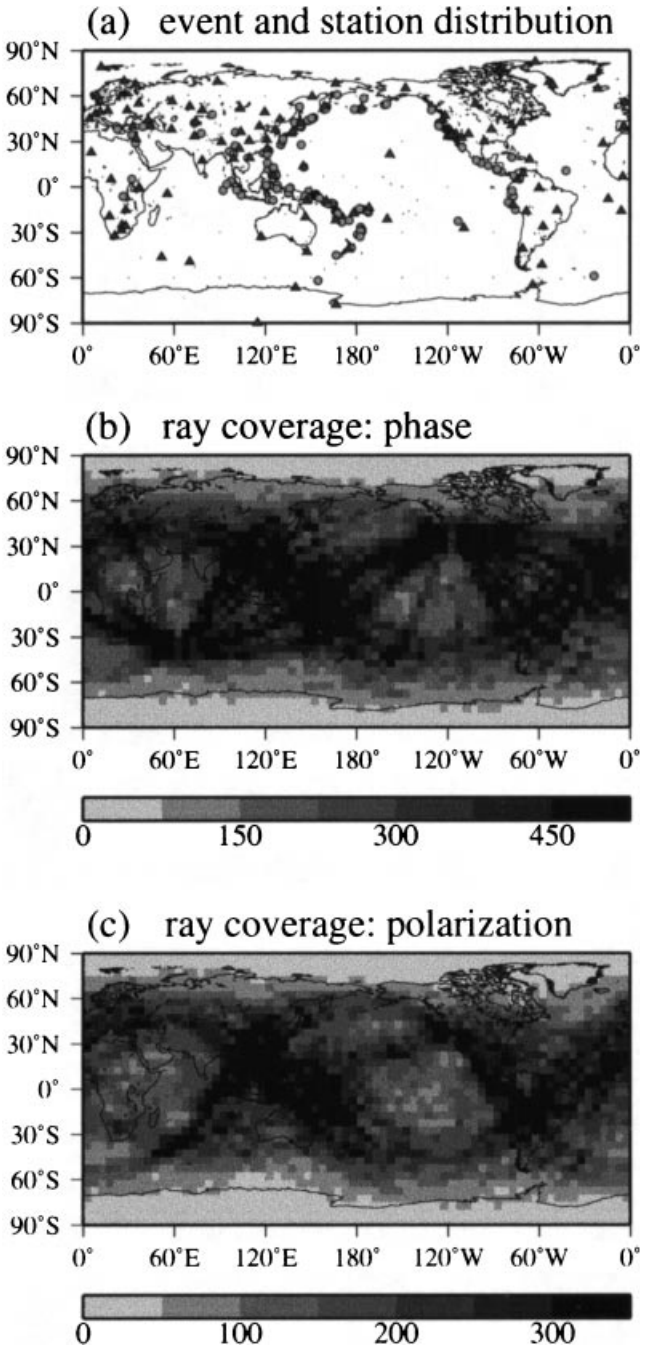

Figure 4. (a) Global distribution of seismic events (circles) from 1990 to 1996 and stations (triangles) used in this study and ray coverage of R1 and R2 for (b) phase data and (c) polarization data at period 152 s. Ray density at each $5° \times 5°$ grid is calculated by counting points along the great-circle path with an interval of 1°. Note that the contour intervals in (b) and (c) are different.

Table 1. The number of phase and polarization data at each period.

	Phase			Polarization		
Period	R1	R2	Total	R1	R2	Total
83 s	2282	1602	3884	1487	648	2135
120 s	2282	1602	3884	1573	950	2523
152 s	2284	1666	3950	1544	958	2502
205 s	2284	1666	3950	1510	943	2453

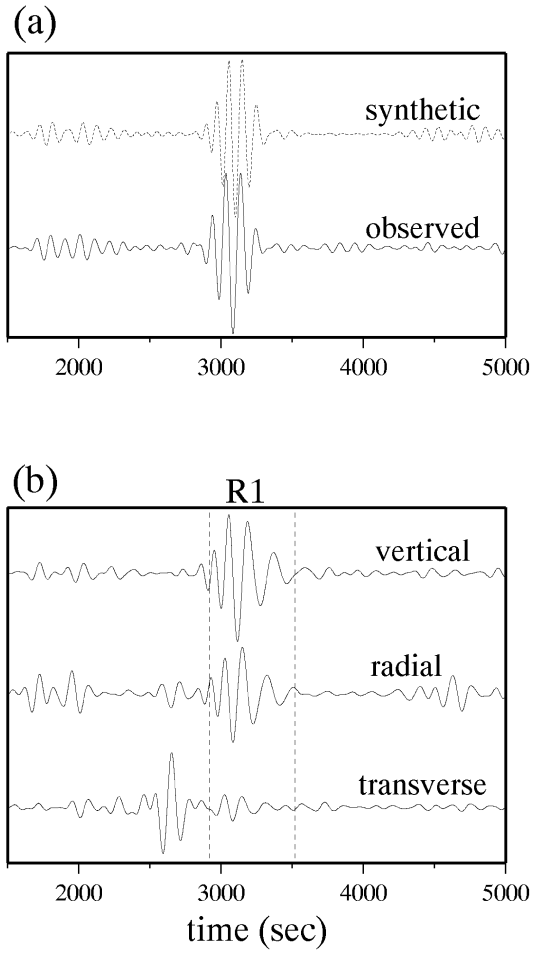

Figure 5. (a) Comparison of observed waveforms (solid line) with synthetic waveforms (dashed line) of the vertical component and (b) three-component seismograms recorded at SBC for an event on 1996 February 17. A bandpass filter is applied (a) between 8 and 12 mHz and (b) between 5 and 12 mHz. Some Rayleigh waves are identified in the transverse component, which indicates the polarization anomaly due to lateral heterogeneities.

We first pick up minor- and major-arc Rayleigh waves (R1 and R2) and apply a bandpass filter to them in the frequency range 4–14 mHz. Next, we calculate their phase differences from corresponding synthetics by using a simple single-station method (e.g. Aki & Richards 1980; Nakanishi & Anderson 1984). We estimate errors in the phase measurements following the technique introduced by Ekström *et al.* (1997). We first assume that each phase measurement contains an error represented by a standard deviation σ of a normal distribution. We then collect all similar-path pairs for which both event and station are located within 3° of each other and calculate the difference in the phase measurements between each pair. If the measurements of each pair are independent, the distribution of phase differences for all possible pairs will have a standard deviation of 2σ. We can thus estimate uncertainty σ in our phase measurement for R1 and R2 at each period independently, although we do not rank each datum as Ekström *et al.* (1997) did.

The polarization angle of each seismogram is analysed by the multitaper method (Park *et al.* 1987a) with four 2.5π-prolate tapers. Detailed procedures of this method were given by Park *et al.* (1987a,b) and Laske *et al.* (1994). We derive three singular values and their corresponding eigenvectors, which represent a 3-D polarization ellipsoid (Fig. 6). If one singular value d_1 is much larger than the other two, d_2 and d_3, the polarization ellipsoid becomes nearly an elliptical plane defined by a complex eigenvector or polarization vector $\hat{\mathbf{z}}$ that corresponds to d_1, which means an ideally polarized Rayleigh wave. After finding the polarization vector $\hat{\mathbf{z}}$, the polarization angle Θ_H is easily estimated from the projected polarization ellipsoid on the horizontal plane (Fig. 6). An example of this analysis is shown in Fig. 7. If the maximum normalized singular value d_1 is smaller than 0.8, its polarization is judged to be unclear and the seismogram is discarded. Measurement errors are estimated from the two minor eigenvectors that correspond to d_2 and d_3, as explained by Park *et al.* (1987a) in detail.

This analysis is also useful for investigating anisotropic features of Rayleigh wave polarization. Polarization anomalies of surface waves are caused not only by lateral heterogeneities but also by azimuthal anisotropy of the Earth (e.g. Crampin 1975; Park & Yu 1992; Yu & Park 1993). It is, however, quite difficult to pinpoint the origin of the observed polarization anomaly in each case. Crampin (1975) described the three types of Rayleigh wave particle motions in anisotropic media with various symmetry conditions. We follow his description and eliminate data that seem to be strongly affected by azimuthal anisotropy. For example, we only choose data that show clearly linear polarization in the horizontal plane (i.e. $\varepsilon_{\mathrm{Rayl}} \approx 1.0$ in Fig. 7c) and the maximum axis of the polarization ellipsoid nearly parallel to the vertical (i.e. $\Theta_V \approx 0.0$ in Fig. 7d).

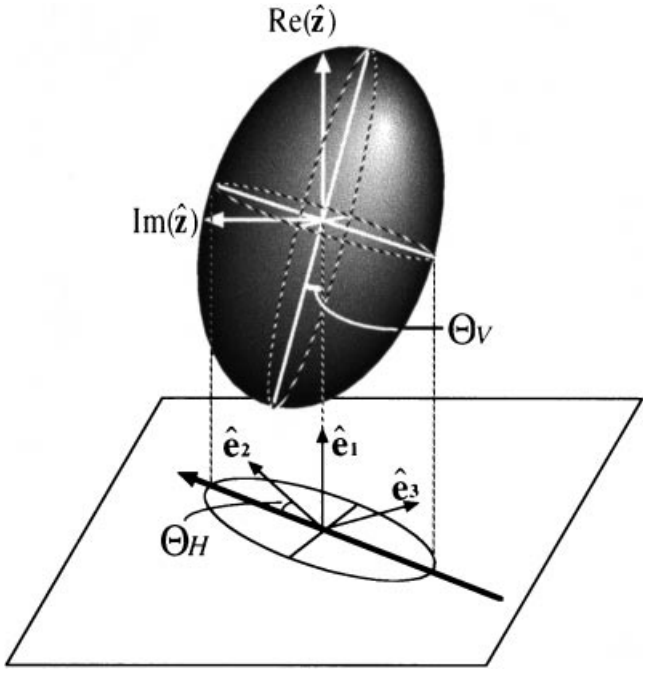

Figure 6. Schematic view of the polarization angle Θ_H measured clockwise from the radial direction $\hat{\mathbf{e}}_2$ in the left-handed coordinate on a horizontal plane in the multitaper polarization analysis. (modified from Park *et al.* 1987a).

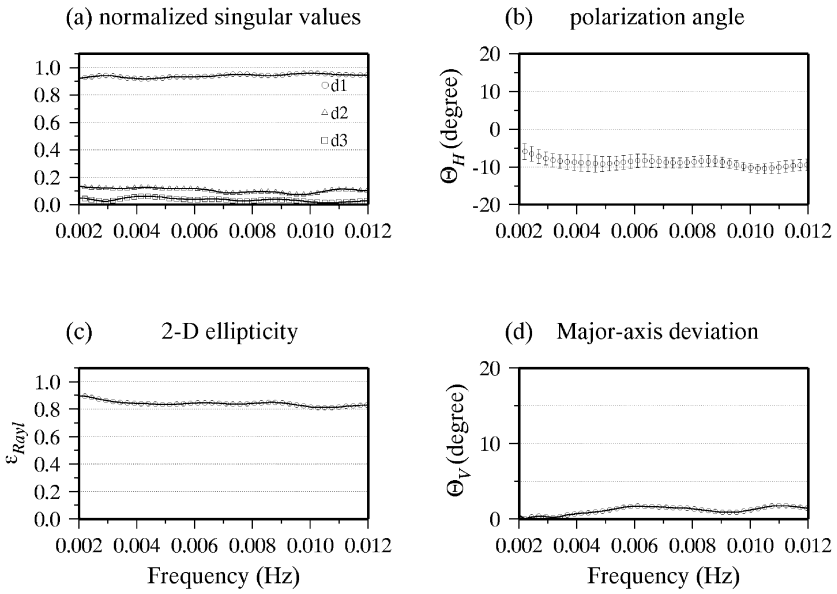

Figure 7. (a) Normalized singular values, (b) polarization angles measured clockwise, (c) ellipticity of the polarization ellipse on the horizontal plane and (d) deviation of the maximum major axis of the polarization ellipsoid from the vertical axis plotted as a function of frequency for the R1 records of Fig. 5(b).

5 STATION CORRECTION

One of the most critical problems in analysing the polarization anomaly from three-component seismograms is the misorientation of seismometers at each station. Some previous studies used surface waves themselves to estimate such misorientations (Laske 1995; Laske & Masters 1996; Larson *et al.* 1997), but it is more desirable to use any independent data for the correction of surface wave arrival angles. In order to estimate the misorientation of each station, we collect direct *P* waves passing through the lower mantle, which is considered to be the least laterally heterogeneous as well as the least anisotropic layer of the Earth for all the seismic phases (Fig. 8). With uniform azimuthal coverage of rays at each station, the distribution of *P*-wave polarization angles, measured from the radial direction, should be a normal distribution with a mean that represents the actual orientation of the seismometers.

Lower-mantle *P*-wave data are collected for events of body wave magnitude greater than 5.1 and focal depth deeper than 30 km from 1990 to 1997, restricting epicentral distances to be larger than 25°. Seismograms are bandpass filtered in the frequency range 15–30 mHz with an average time window of 70 s. Picking up the first motion of *P* waves would be the most suitable way to estimate *P*-wave arrival angles, but actual long-period *P*-wave records do not show a sharp first motion. We therefore pick up the first one or two wavelengths of *P* waveforms in the above time window (Fig. 9a). In such a short time window with a sampling interval of 1 s, we cannot make any optimal tapers, so that the multitaper method used for Rayleigh waves is not suitable for long-period *P* waves. Instead, we use complex polarization analysis in the time domain (Vidale 1986), assuming that *P*-wave polarization is independent of frequency, not dispersive like surface waves. In other words, its arrival angle is expected to be constant in the chosen time window, although the actual measurements show a slight time dependence (Fig. 9b), from which we can estimate errors in our measurements. Ellipticity of polarization in the horizontal plane is also used to evaluate the accuracy of the measured arrival angles (Fig. 9c) because it should be straight for ideal *P* waves ($\varepsilon_P \approx 1.0$).

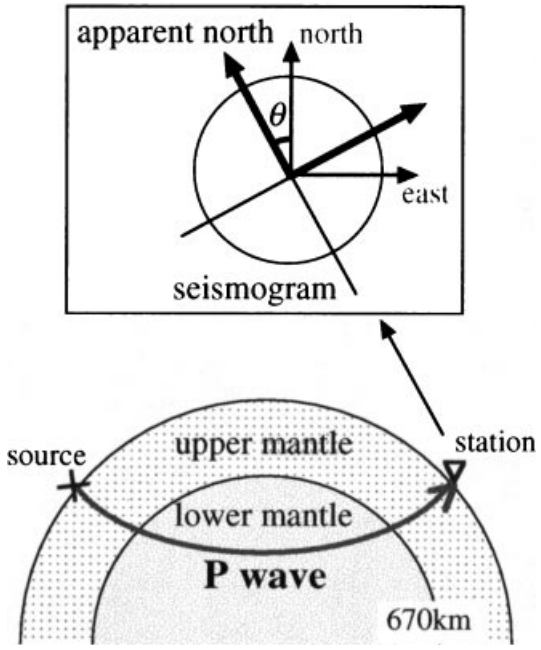

Figure 8. Schematic view of station correction measured by lower-mantle *P*-wave polarization.

In most stations, the distribution of *P*-wave polarization angles is fitted with a normal distribution, as shown in Fig. 10. Stations located in subduction regions such as MAJO and SNZO show larger variances than those on stable continents such as CTAO and NWAO. Considering the tectonic setting of these stations, lateral heterogeneities in the upper mantle due to subducting slabs may affect the polarization of long-period

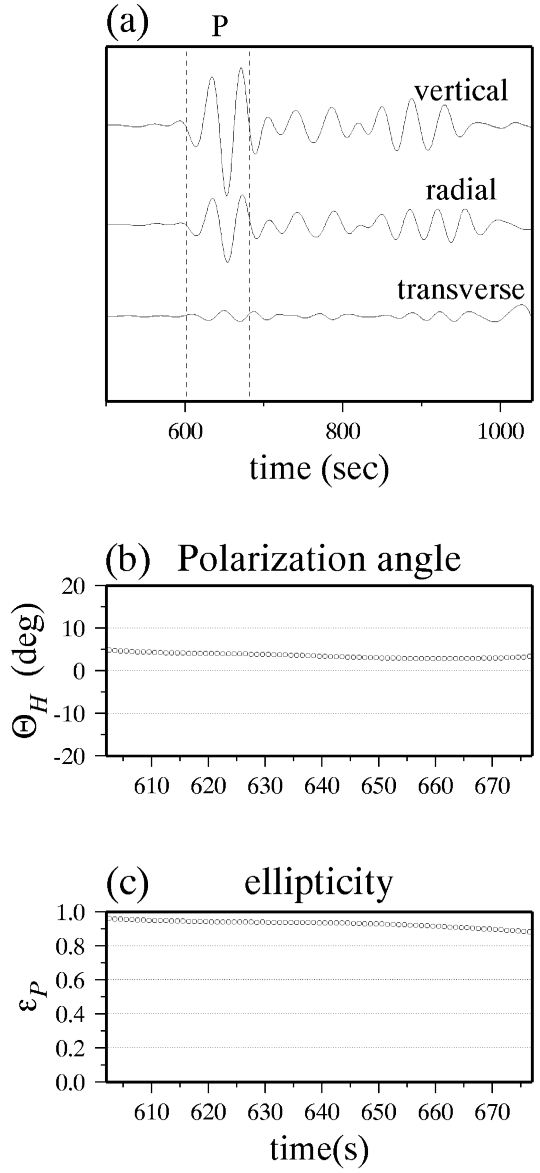

Figure 9. Polarization analysis of lower-mantle *P* wave recorded at ANMO for an event of 1992 March 2. (a) Three-component seismogram, (b) polarization angles measured clockwise (estimated arrival angle of this seismogram is $3.92 \pm 0.12^\circ$) and (c) ellipticity of polarization ellipse on the horizontal plane plotted as a function of time.

P waves much more than previously expected (e.g. Woodward & Masters 1991), which is worthy of further investigation in the future. The station misorientations are defined by taking the mean value of the arrival angles for each station. As pointed out in previous works (Laske 1995; Laske & Masters 1996; Larson *et al.* 1997), some stations such as AAK, NWAO, TATO and SNZO show large misalignments in horizontal components, although in most stations misalignments are less than 4°. Our results are compared with the estimates of Laske & Masters (1996) in Table 2. Note that their results were originally provided in the right-handed coordinate system; we therefore corrected them to the left-handed system, resulting in positive deviation from the north representing the misalignment to the east. In spite of the completely different data sets, the estimated misorientations in this study are quite consistent with those of Laske & Masters (1996), especially for stations with a large misorientation.

Table 2. Comparison of estimated misorientations in this study with those of Laske & Masters (1996) at six stations. All the misorientations are measured clockwise with the unit in degrees so that a positive deviation represents the misalignment of a seismometer to the east. Numbers in parentheses show the number of data used to estimate misorientations.

	This study (*P* waves)	Laske & Masters (surface waves)
AAK	6.58 ± 1.42(49)	6.84 ± 0.59(104)
MAJO	-3.15 ± 0.89(226)	-6.00 ± 0.45(176)
NWAO	4.61 ± 0.71(201)	4.70 ± 1.20(40)
SNZO	5.59 ± 1.75(82)	4.57 ± 0.64(81)
TATO	-13.21 ± 1.51(79)	-9.90 ± 1.83(29)
TLY	3.59 ± 1.10(80)	3.71 ± 0.57(74)

6 APPLICATION TO THE OBSERVED RAYLEIGH WAVE DATA

We apply the actual phase or polarization data of Rayleigh waves to the linear inversion after the station correction. The phase velocity maps obtained are shown in Fig. 11, and their amplitude spectra and correlation coefficients in Fig. 12. These models are expanded in spherical harmonics up to degree 15. Data misfits for phase or polarization data at each period are listed in Table 3. The misfit derived from the polarization data inversion is generally smaller than that from the phase for all periods because of the larger estimated errors of the polarization data.

In the phase data models (on the left of Fig. 11), low-velocity anomalies exist along the East Pacific Rise, near the Red Sea rift zone and near Iceland, whilst high-velocity anomalies exist in the Canadian and Siberian shields, Australia and the western Pacific. These characteristics are in good agreement with some geological information; for example, there are high-velocity anomalies in shields and old oceanic basins associated with plate cooling, whilst low-velocity anomalies occur in some regions of high tectonic activity such as hot spots and ridges.

Comparison of our phase-data model with another two models, the Scripps model from both phase and polarization data (Laske & Masters 1996) and the Harvard model from phase data (Ekström *et al.* 1997), at a period of 100 s is shown in Fig. 13. Other models derived from phase data (e.g. Zhang & Lay 1996) are nearly identical to these models, especially at low orders. These models were expanded in spherical harmonics up to degrees 24 for the Scripps model and 40 for the Harvard model, but their spatial distributions agree well with each other, suggesting that higher-order heterogeneities do not alter the general appearance of these phase velocity maps,

Table 3. Data misfits of phase and polarization data inversions at each period.

	83 s	120 s	152 s	205 s
Phase	12.0	5.0	5.0	4.5
Polarization	5.0	2.9	2.3	3.1

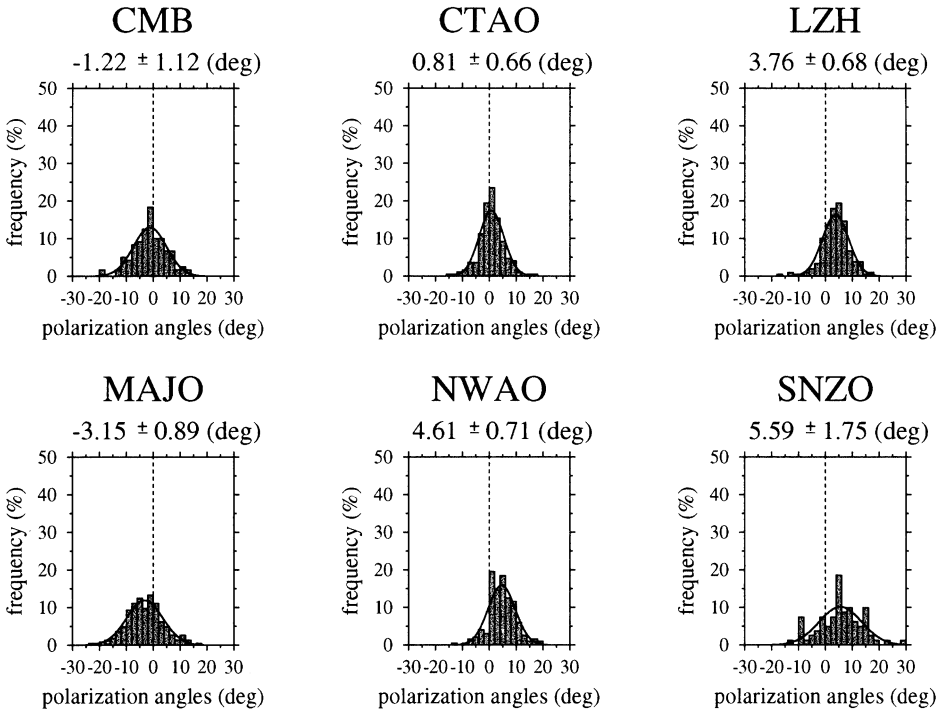

Figure 10. Distributions of *P*-wave arrival angles at six stations. Solid lines show a least-squares-fitted normal distribution, the abscissa is the polarization angle from the radial direction (0 degree) and the ordinate represents the frequency of data. Arrival angles are measured clockwise. The number under each station name shows the estimated misorientation.

although higher orders are important for describing small-scale structures. Fig. 14 shows a comparison of amplitude spectra and the correlation amongst these models up to degree 15. The spectra of our model are somewhat smaller at low orders, especially at degrees 1–3, than the other models. The correlation amongst these models is quite good for low orders up to 6 and falls gradually at higher orders. In spite of such slight discrepancies, variations of spectral amplitude share a fairly common overall trend (for example, characteristic peaks at degrees 2 and 5), which seems to justify our present model from phase data.

The polarization data models (on the right of Fig. 11) also show some agreement with geological information, such as high-velocity anomalies in North America, Siberia, western Australia and the western Pacific, and low-velocity anomalies in the eastern Pacific and eastern Africa. However, there are several apparent discrepancies between the phase and polarization models, for example a low-velocity anomaly in the Indian Ocean and a high-velocity anomaly in the southern Pacific. Comparatively sparse path coverage in some regions (that is, the eastern region of Africa and the southeastern Pacific, as seen in Fig. 4c) may be one of the main reasons for these discrepancies. In addition, the observed polarization data seem to contain more noise than the phase data owing to the difficulty of making polarization measurements from three-component seismograms, as discussed in the previous section.

The correlation between the phase and polarization models at each period (Fig. 12c) is especially good for low even degrees (i.e. degrees 2, 4 and 6) and generally bad for low odd degrees and for degrees higher than 8. A similar trend has already been reported by Laske (1995) and this may also justify our polarization models. These low even degrees, especially degrees 2 and 6, have been discussed in relation to the upper-mantle structure (e.g. Nakanishi & Anderson 1984; Richards *et al.* 1988; Montagner & Romanowicz 1993; Zhang & Lay 1996): the degree 2 anomaly is generally discussed in connection with geoid highs and the degree 6 with the distribution of hotspots. Considering the characteristics of these low even degrees and their good correlation, it is likely that these geological features in the upper mantle have considerable influence on both phase and polarization data.

In contrast, except for 83 s, our polarization data models do not show a remarkable amplitude at degree 5 that is clearly seen in our phase data model, particularly at shorter periods (82 and 120 s in Fig. 12a). In addition, the correlation at degree 5 is not good. Some previous studies with phase data have discussed the fact that the pattern of degree 5 agrees quite well with the distribution of shields, old oceans and ridges (e.g. Zhang & Lay 1996). The disagreement between our phase and polarization models at degree 5 suggests that shallow structures such as continental crust or ridges do not have a significant effect on our polarization data. Taking the different sensitivities to velocity perturbations (i.e. 1 and 2) into account, it is probable that such shallow structures have quite sharp boundaries (e.g. continent–ocean boundary) without much velocity gradient, and, consequently, they mainly appear in the phase models, not in the polarization models.

Almost all the previous phase velocity models derived only from phase data have a spectral peak at degree 2 and their spectra rapidly fall off proportional to l^{-1} or l^{-2} (e.g. Zhang & Tanimoto 1991; Su & Dziewonski 1992; Passier & Snieder 1995; Zhang & Lay 1996). This trend is also seen in both phase and polarization models in this study (Fig. 12). Whilst polarization

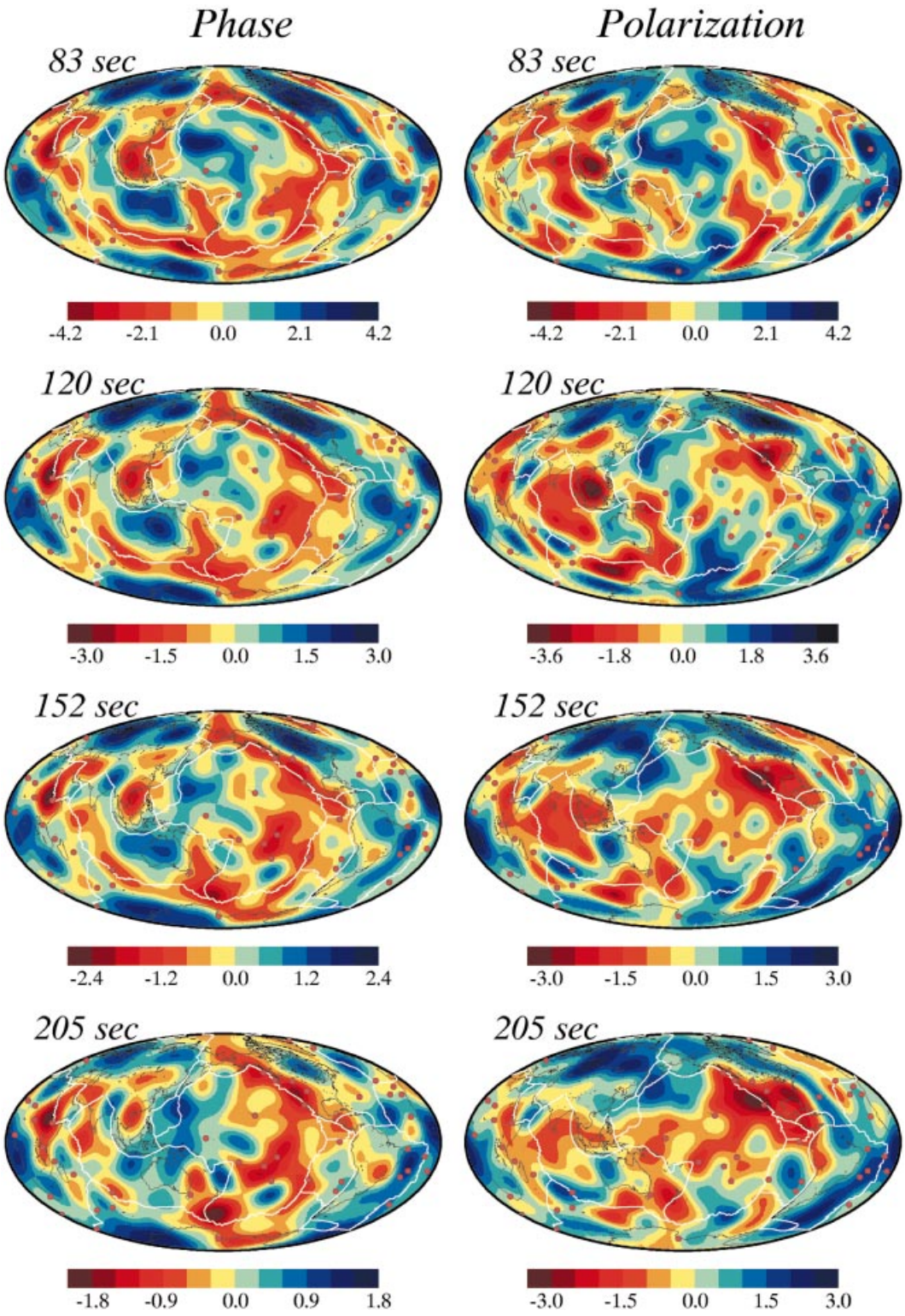

Figure 11. Phase velocity maps using phase and polarization data at 83, 120, 152 and 205 s. Red areas represent low-velocity regions whilst blue areas represent high-velocity regions. Red circles represent the locations of hotspots (Richards *et al.* 1988).

data should be more sensitive to higher-order heterogeneities, we cannot apparently see the improved sensitivity to higher orders in our polarization models (Fig. 12b). This may be caused by the weighting applied to the model parameters in the process of inversion to avoid aliasing effects due to the truncation of spherical harmonics.

In order to investigate spectral characteristics at higher orders in detail, we pay attention only to the amplitude spectra higher than degree 6. In this range of harmonic degrees, amplitude spectra from the polarization data systematically show smaller gradients than those from phase data (Fig. 15a and Table 4) at all periods, supporting the idea that the polarization

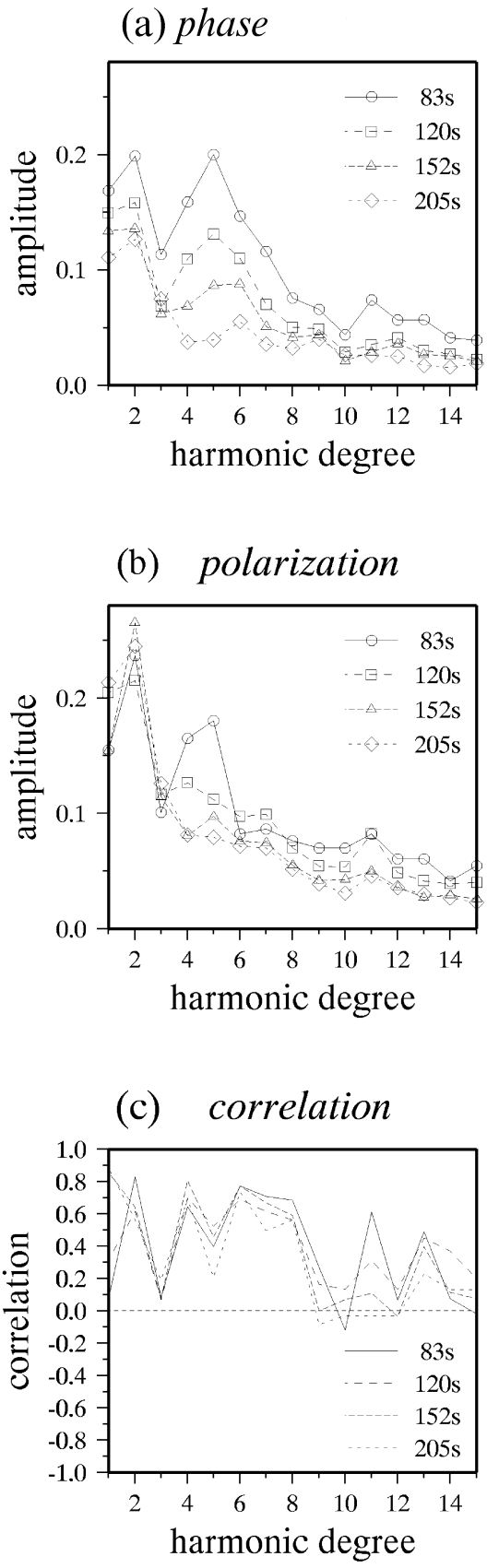

Figure 12. Amplitude spectra of phase velocity maps using (a) phase data and (b) polarization data and (c) their correlation at each period. Circles, squares, triangles and diamonds represent the spectra at 83, 120, 152 and 205 s, respectively.

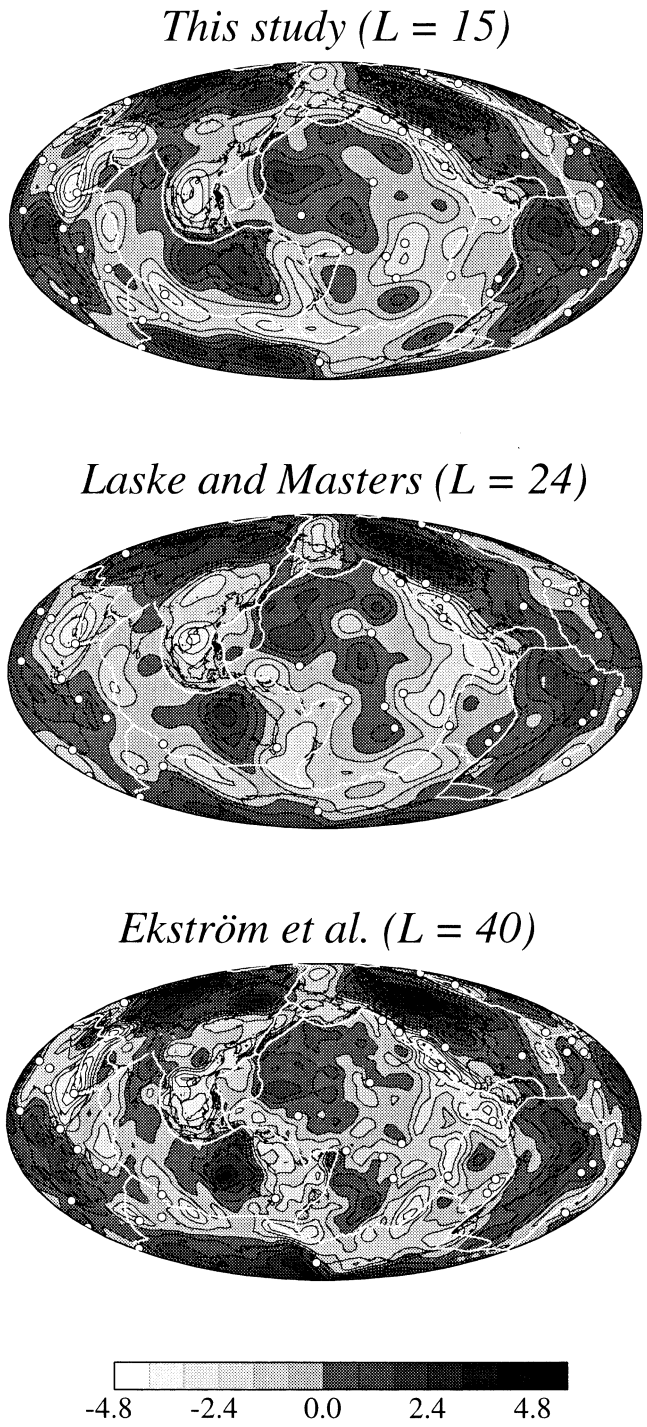

Figure 13. Comparison of our phase velocity map (top) using phase data of Rayleigh waves at a period of 100 s with those of Laske & Masters (1996) (middle) and Ekström *et al.* (1997) (bottom).

data possess slightly greater sensitivity to higher orders than the phase data. From this result, one may ask whether the gradient of higher-order spectra is controlled by the choice of damping. We therefore perform inversions with underdamping and overdamping to find a possible range of spectra for each model (Fig. 15b). The underdamped model gives the minimum gradient at each period whilst the overdamped model gives the maximum. The under- and overdamped solutions are

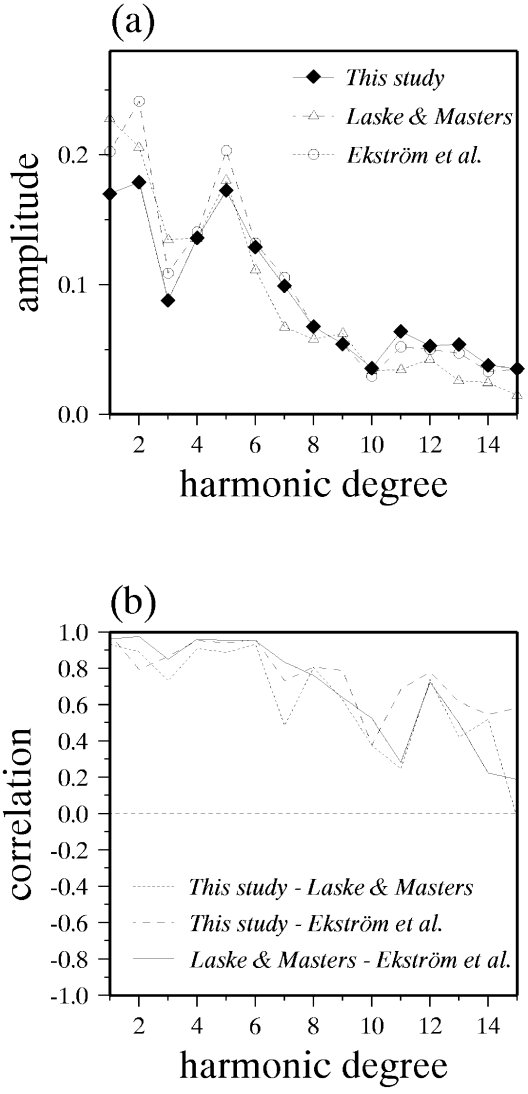

Figure 14. (a) Comparison of amplitude spectra and (b) correlation amongst the three phase velocity maps of Fig. 13. Diamonds, triangles and circles represent the amplitude spectra of this study, those of Laske & Masters (1996) and those of Ekström *et al.* (1997), respectively.

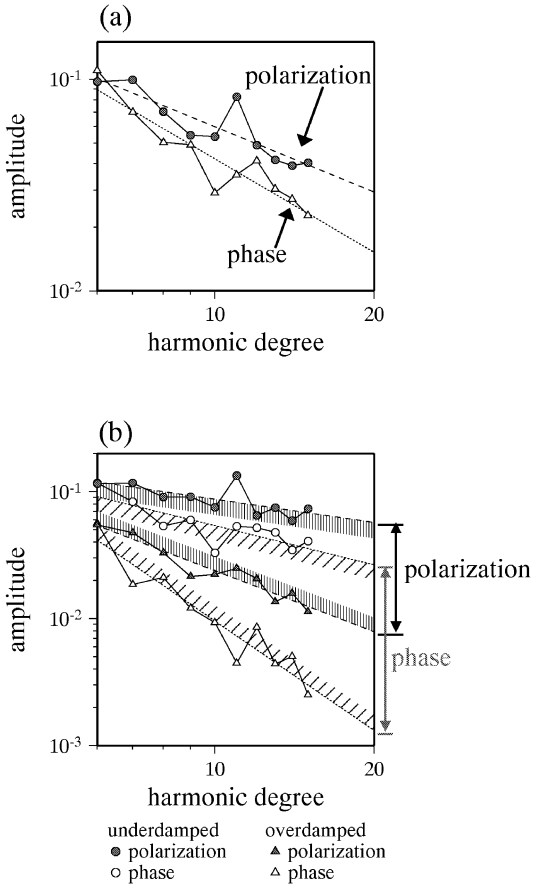

Figure 15. (a) Amplitude spectra of our phase velocity models (120 s, Fig. 12) for $l \geq 6$ in a logarithmic plot. Straight lines are least-squares fitted lines. (b) Same as (a) except for underdamped (circles) and overdamped (triangles) inversion models. Shaded areas show possible ranges within which the amplitude spectra are expected to vary with different damping parameters.

subjectively chosen from the trade-off diagram (Fig. 2). A reasonable damping should be located in the range of both. The gradients of spectral variation from polarization data are obviously smaller than those from the phase data, as shown in Table 4, especially at shorter periods such as 83 and 120 s. In the long-period range (more than 152 s), the difference in spectral gradients becomes small. The longer the period, the longer the wavelength of the surface waves becomes. Therefore, it is reasonable that the resolving power of both phase and polarization data for high-order heterogeneities becomes weak and their differences become less apparent as the period increases.

Su & Dziewonski (1991) suggested that the significantly large anomaly of degree 2 shown in previous studies (e.g. Masters *et al.* 1982) should characterize the most dominant feature of the actual Earth and concluded that large-scale lateral heterogeneities are dominant in the mantle. On the

Table 4. Indices x of the gradient of amplitude spectra (l^{-x}, where l is the degree of spherical harmonics) for underdamped, reasonably damped and overdamped inversions at each period.

	82 s		120 s		152 s		205 s	
	Phase	Pol.	Phase	Pol.	Phase	Pol.	Phase	Pol.
Underdamping	1.0	0.3	1.0	0.6	0.8	0.7	0.8	0.9
Reasonable damping	**1.3**	**0.6**	**1.5**	**1.0**	**1.3**	**1.2**	**1.2**	**1.2**
Overdamping	2.6	1.1	2.9	1.6	2.9	1.6	3.2	1.5

other hand, a remarkable discrepancy in higher-order spectra between global and regional models was reported by Passier & Snieder (1995), and they concluded that the actual Earth probably contains more spectral power around degree 30 than is present in previous global models. As one of the reasons for this discrepancy, they mentioned that higher-orders in global models are underestimated due to the limited path coverage. The suppression of higher orders caused by path integration was discussed in previous studies. For example, Kawakatsu (1983) concluded that the averaging property of great-circle data reduces the resolution of heterogeneities in inversion, and Mochizuki (1993) computed the resolving sensitivity of line integrals to lateral heterogeneity, based on geometrical ray theory, assuming that ray paths are random. He showed that sensitivity to higher orders generally decreases with increasing harmonic degrees and in particular is greater for even orders than for odd orders when major-arc wave trains (R2 or G2) are included in the data set.

Since we use both actual phase and actual polarization data within the framework of geometrical ray theory and all the data are approximated by line integration along great-circle paths (see 1 and 2), the low-pass effect of this approximation may play a crucial role in inversions for both phase and polarization data. Moreover, the actual path coverage is rather uneven (Fig. 4), which results in a biased spatial resolution of heterogeneities, and this may also emphasize the low-pass effect. As a result, the inverted models may have a similar trend for both kinds of data; that is, low-order heterogeneities are remarkable and higher-order spectra are suppressed (Fig. 12).

To prove the influence of uneven path coverage on the higher orders, we recall the synthetic test with a white noise model discussed in Section 3. We perform another synthetic test by using about 4000 ray paths of the actual phase data (Fig. 4b), although the number of paths is slightly smaller than the number of synthetic paths (4600 paths). The retrieved models from the synthetic phase and polarization data sets are shown in Figs 3(f) and (g). Higher-order amplitude spectra of both phase and polarization models, particularly higher than degree 8, are clearly suppressed, whereas the previous synthetic test with polarization data with sufficiently dense and even paths (Fig. 3c) shows almost complete retrieval for higher-order heterogeneities of the original model. The only different factor in the process of retrieving the models shown in Figs 3(b) and (c) and Figs 3(g) and (f) is the ray coverage, so that it is reasonable to conclude that the reduced amplitude of retrieved models at higher degrees seen in Figs 3(g) and (f) is caused by the uneven coverage of the actual ray paths. It is also important to note that the amplitude spectra retrieved from polarization data (Fig. 3g) have slightly larger amplitudes at higher degrees than those from phase data (Fig. 3f), which also suggests the greater sensitivity of polarization data to higher-order heterogeneities.

Even if we use polarization data and suppose that there exist more significant higher-order heterogeneities in the mantle than have ever been proposed, the above results indicate that we may not be able to extract small-scale heterogeneities from the observed data sufficiently well due to the path-averaging effect of uneven paths as long as we adopt the ray theoretical approach. Consequently, the results of the synthetic and actual data inversions in this study may exhibit the limit of the ray theoretical approaches to retrieve higher-order heterogeneities. Even though our polarization models show slightly larger amplitudes at higher orders than the phase models, we may need to consider path deviations from great-circle paths in interpreting polarization data. As another possible approach to enhance the resolving power for higher orders, integration over areas of finite width along geometrical rays may be useful (Yomogida & Aki 1987) for taking the effect of finite wavelengths into consideration.

7 CONCLUSIONS

We performed linear inversions, first using the synthetic phase or polarization data with a white noise model, and showed the intrinsic resolving power of the polarization data for higher-order heterogeneities compared with that of the phase data. This result indicates the possibility of enhancing the resolution of tomographic models by the introduction of polarization data, as pointed out by Laske & Masters (1996). The synthetic test clearly suggests that polarization data are able to retrieve small-scale heterogeneities more reliably than phase data if path coverage is sufficiently dense and uniform with high-quality data, whilst higher orders retrieved from phase data may be easily suppressed by damping or smoothing effects, in spite of a reasonable damping. Furthermore, polarization data are likely to be able to retrieve not only higher orders but also lower orders well. Since this test uses synthetic paths that correspond to minor-arc wave trains with sufficiently dense and uniform path coverage, actual polarization data may also be able to provide some important information on the intensity of higher-order heterogeneities in the real Earth if we use high-quality minor-arc wave data (R1 or G1) with ideal path coverage in the future.

We inverted the observed phase or polarization data of long-period Rayleigh waves for phase velocity models. We also estimated the misorientation of each station from the observed polarization anomaly of lower-mantle *P* waves as independent information. Some stations such as AAK, NWAO, SNZO and TATO show significant deviation from the reported N–S direction, and the estimated misorientations are quite consistent with the previous result of Laske & Masters (1996), in spite of completely different kinds of data. The correlation between the phase velocity models from phase and polarization data is quite good for low even degrees, but not for low odd degrees and degrees higher than 8. A comparison of their spectra shows that our polarization data are able to resolve low even orders sufficiently, and bad correlations in low odd orders such as 3 and 5 (Fig. 12c) are mainly responsible for the discrepancies between these models. The path coverage of our present data set appears to be enough to retrieve a reliable model that is expanded in spherical harmonics up to degree 15, but the uneven path coverage would reduce the resolving power for higher orders even if we used polarization data. Although the difference in higher-order amplitude spectra between phase and polarization models is not so significant, the polarization data models show slightly larger amplitudes at higher orders and a smaller gradient of spectral variation than the phase data, especially for short periods such as 83 and 120 s, considering a reasonable range of damping effects. In addition to the results of the synthetic test, these characteristics in polarization models also support the idea that polarization data are indeed more helpful in retrieving small-scale structures than phase data. At the same time, the similar overall trends in our phase and polarization models and in the result of

the additional synthetic test with the actual uneven paths, which are based on the geometrical ray theory, suggest the limited resolving power for higher-order heterogeneities with the present conditions of global data.

When we use polarization data, we must pay attention to some other important factors. For example, polarization data cannot resolve the global average of phase velocity (i.e. degree 0 in spherical harmonics), since they reflect the averaged derivation of phase velocity perturbations. If it is necessary to consider the magnitude of velocity perturbations from the reference earth model, joint inversions with phase data will be essential. In addition, we need excellent S/N ratios of three-component seismograms, and epicentral distances should be longer than 50° to avoid the overlapping of other signals, resulting in smaller amounts of polarization data and poorer coverage than phase data with the same criteria. As another important effect on polarization data, we should not overlook azimuthal anisotropy in the upper mantle (Laske & Masters 1998; Larson *et al.* 1998), although general consensus on the degree of azimuthal anisotropy on a global scale has not yet been attained. Nevertheless, these difficulties are expected to be overcome by the increasing number of seismic stations with high-precision seismometers in the near future.

ACKNOWLEDGMENTS

We thank Gabi Laske and Erik Larson for their critical and helpful comments on an earlier version of the manuscript. We are also grateful to Göran Ekström and Gabi Laske for making their tomography models available to us. We also thank two anonymous reviewers and the editor Brian Kennett for their helpful and constructive comments. We would like to give special thanks to all the groups operating the Global Seismographic Network for providing us with the huge amounts of high-quality data used in this study. This study was partly supported by the Earthquake Research Institute (University of Tokyo) cooperative research program (1996-G0-05) and by Grant-in-Aid for Scientific Research (C) (No. 10640409), sponsored by the Ministry of Education, Science and Culture of Japan. The first author was supported by a JSPS Research Fellowship for Young Scientists.

REFERENCES

Aki, K. & Richards, P.G., 1980. *Quantitative Seismology, Theory and Methods,* Vol. II, W. H. Freeman, San Francisco.

Backus, G.E., 1964. Geographical interpretation of measurements of average phase velocities of surface waves over great circular and great semi-circular paths, *Bull. seism. Soc. Am.,* **54,** 571–610.

Boore, D.M., 1969. Effect of higher mode contamination on measured Love wave phase velocities, *J. geophys. Res.,* **74,** 6612–6616.

Crampin, S., 1975. Distinctive particle motion of surface waves as a diagnostic of anisotropic layering, *Geophys. J. R. astr. Soc.,* **40,** 177–186.

Doornbos, D.J., 1988. Asphericity and ellipticity corrections, in *Seismological Algorithms,* pp. 75–85, ed. Doornbos, D.J., Academic Press, London.

Dziewonski, A.M., 1984. Mapping the lower mantle: determination of lateral heterogeneity in *P* velocity up to degree and order 6, *J. geophys. Res.,* **89,** 5929–5952.

Dziewonski, A.M. & Anderson, D.L., 1981. Preliminary reference Earth model, *Phys. Earth planet. Inter.,* **25,** 297–356.

Dziewonski, A.M. & Woodhouse, J.H., 1983. Studies of the seismic source using normal-mode theory, in *Earthquakes: Observation, Theory and Interpretation,* pp. 45–137, eds Kanamori, H. & Boschi, E., North-Holland, Amsterdam.

Dziewonski, A.M., Miles, J. & Bloch, S., 1972. Residual dispersion measurement—a new method of surface-wave analysis, *Bull. seism. Soc. Am.,* **62,** 129–139.

Dziewonski, A.M., Chou, T.-A. & Woodhouse, J.H., 1981. Determination of earthquake source parameters from waveform data for studies of global and regional seismicity, *J. geophys. Res.,* **86,** 2825–2852.

Ekström, G., Tromp, J. & Larson, E.W.F., 1997. Measurements and global models of surface wave propagation, *J. geophys. Res.,* **102,** 8137–8157.

Hara, T., Tsuboi, S. & Geller, R.J., 1993. Inversion for laterally heterogeneous upper mantle *S*-wave velocity structure using iterative waveform inversion, *Geophys. J. Int.,* **115,** 667–698.

Honda, S. & Tanimoto, T., 1987. Regional 3-D heterogeneities by waveform inversion—application to the Atlantic area, *Geophys. J. R. astr. Soc.,* **91,** 737–753.

Inoue, H., Fukao, Y., Tanabe, K. & Ogata, Y., 1990. Whole mantle P-wave travel time tomography, *Phys. Earth planet. Inter.,* **59,** 294–328.

Kawakatsu, H., 1983. Can 'pure-path' models explain free oscillation data?, *Geophys. Res. Lett.,* **10,** 186–189.

Kennett, B.L.N., Widiyantoro, S. & van der Hilst, R.D., 1998. Joint seismic tomography for bulk sound and shear wave speed in the Earth's mantle, *J. geophys. Res.,* **103,** 12 469–12 493.

Larson, E.W.F., Ekstöm, G. & Tromp, J., 1997. Analysis of surface wave arrival angle measurements, *EOS, Trans. Am. geophys. Un.,* **78,** F484 (abstract).

Larson, E.W.F., Tromp, J. & Ekström, G., 1998. Effects of slight anisotropy on surface waves, *Geophys. J. Int.,* **132,** 654–666.

Laske, G., 1995. Global observation of off-great-circle propagation of long-period surface waves, *Geophys. J. Int.,* **123,** 245–259.

Laske, G. & Masters, G., 1996. Constraints on global phase velocity maps from long-period polarization data, *J. geophys. Res.,* **101,** 16 059–16 075.

Laske, G. & Masters, G., 1998. Surface-wave polarization data and global anisotropic structure, *Geophys. J. Int.,* **132,** 508–520.

Laske, G., Masters, G. & Zürn, W., 1994. Frequency-dependent polarization measurements of long-period surface waves and their implications for global phase-velocity maps, *Phys. Earth planet. Inter.,* **84,** 111–137.

Lay, T. & Kanamori, H., 1985. Geometric effects of global lateral heterogeneity on long-period surface wave propagation, *J. geophys. Res.,* **90,** 605–621.

Masters, G., Jordan, T.H., Silver, P.G. & Gilbert, F., 1982. Aspherical Earth structure from fundamental spheroidal-mode data, *Nature,* **298,** 609–613.

Mochizuki, E., 1993. Spherical harmonic analysis in terms of line integral, *Phys. Earth planet. Inter.,* **76,** 97–101.

Montagner, J.-P. & Romanowicz, B., 1993. Degree 2, 4, 6, inferred from seismic tomography, *Geophys. Res. Lett.,* **20,** 631–634.

Montagner, J.-P. & Tanimoto, T., 1990. Global anisotropy in the upper mantle inferred from the regionalization of phase velocities, *J. geophys. Res.,* **95,** 4797–4819.

Nakanishi, I. & Anderson, D.L., 1983. Measurements of mantle wave velocities and inversion for lateral heterogeneity and anisotropy, 1. Analysis of great circle phase velocities, *J. geophys. Res.,* **88,** 10 267–10 283.

Nakanishi, I. & Anderson, D.L., 1984. Measurements of mantle wave velocities and inversion for lateral heterogeneity and anisotropy, 2. Analysis by the single-station method. *Geophys. J. R. astr. Soc.,* **78,** 573–617.

Neele, F., VanDecar, J.C. & Snieder, R.K., 1993. The use of P-wave amplitude data in joint inversions with travel times for upper-mantle velocity structure, *J. geophys. Res.,* **98,** 12 033–12 054.

Park, J. & Yu, Y., 1992. Anisotropy and coupled free oscillations: simplified models and surface wave observations, *Geophys. J. Int.,* **110,** 401–420.

Park, J., Vernon, F.L. & Lindberg, C.R., 1987a. Frequency dependent polarization analysis of high-frequency seismograms, *J. geophys. Res.,* **92,** 12 664–12 674.

Park, J., Lindberg, G.R. & Vernon, F.L., 1987b. Multitaper spectral analysis of high-frequency seismograms, *J. geophys. Res.,* **92,** 12 675–12 684.

Passier, M.L. & Snieder, R.K., 1995. On the presence of intermediate-scale heterogeneity in the upper mantle, *Geophys. J. Int.,* **123,** 817–837.

Richards, M.A., Hager, G.H. & Sleep, N.H., 1988. Dynamically supported geoid highs over hotspots: observation and theory, *J. geophys. Res.,* **93,** 7690–7708.

Su, W.-J. & Dziewonski, A.M., 1991. Predominance of long-wavelength heterogeneity in the mantle, *Nature,* **352,** 121–126.

Su, W.-J. & Dziewonski, A.M., 1992. On the scale of mantle heterogeneity, *Phys. Earth planet. Inter.,* **66,** 160–202.

Su, W.-J., Woodward, R.L. & Dziewonski, A.M., 1994. Degree-12 model of shear-velocity heterogeneity in the mantle, *J. geophys. Res.,* **99,** 6945–6980.

Tanimoto, T., 1990. Long-wavelength S-wave velocity structure throughout the mantle, *Geophys. J. Int.,* **100,** 327–336.

Tanimoto, T. & Anderson, D.L., 1985. Lateral heterogeneity and azimuthal anisotropy of the upper mantle: Love and Rayleigh waves 100–250 s, *J. geophys. Res.,* **90,** 1842–1858.

Thatcher, W. & Brune, J.N., 1969. Higher mode interference and observed anomalous apparent Love wave phase velocities, *J. geophys. Res.,* **74,** 6603–6611.

Trampert, J. & Woodhouse, J.H., 1995. Global phase velocity maps of Love and Rayleigh waves between 40 and 150 seconds, *Geophys. J. Int.,* **122,** 675–690.

Vidale, J.E., 1986. Complex polarization analysis of particle motion, *Bull. seism. Soc. Am.,* **76,** 1393–1405.

Woodhouse, J.H. & Dziewonski, A.M., 1984. Mapping the upper mantle: three-dimensional modeling of Earth structure by inversion of seismic waveforms, *J. geophys. Res.,* **89,** 5953–5986.

Woodhouse, J.H. & Wong, Y.K., 1986. Amplitude, phase and path anomalies of mantle waves, *Geophys. J. R. astr. Soc.,* **87,** 753–773.

Woodward, R.L. & Masters, G., 1991. Global upper mantle structure from long-period differential travel times, *J. geophys. Res.,* **96,** 6351–6377.

Yanovskaya, T.B., 1996. Ray tomography based on azimuthal anomalies, *Pure appl. Geophys.,* **148,** 319–336.

Yomogida, K. & Aki, K., 1987. Amplitude and phase data inversion for phase velocity anomalies in the Pacific Ocean basin, *Geophys. J. R. astr. Soc.,* **88,** 161–204.

Yu, Y. & Park, J., 1993. Upper mantle anisotropy and coupled-mode long-period surface waves, *Geophys. J. Int.,* **114,** 473–489.

Zhang, Y.-S. & Lay, T., 1996. Global surface wave phase velocity variations, *J. geophys. Res.,* **101,** 8415–8436.

Zhang, Y.-S. & Tanimoto, T., 1991. Global Love wave phase velocity and its significance to plate tectonics, *Phys. Earth planet. Inter.,* **66,** 160–202.